Research Article | Vol. 9, No. 8 | 1 Aug 2018 | BIOMEDICAL OPTICS EXPRESS 3725
Biomedical Optics EXPRESS

Optofluidic detection of Zika nucleic acid and protein biomarkers using multimode interference multiplexing

ALEXANDRA STAMBAUGH,[1,*] JOSHUA W. PARKS,[1] MATTHEW A. STOTT,[2] GOPIKRISHNAN G. MEENA,[1] AARON R. HAWKINS,[2] AND HOLGER SCHMIDT[1]

[1]*School of Engineering, University of California, Santa Cruz, 1156 High St., Santa Cruz, CA 95064, USA*
[2]*ECEn Department, Brigham Young University, 459 Clyde Building, Provo, UT 84602, USA*
**amstamba@ucsc.edu*

Abstract: The recent massive Zika virus (ZIKV) outbreak illustrates the need for rapid and specific diagnostic techniques. Detecting ZIKV in biological samples poses unique problems: antibody detection of ZIKV is insufficient due to cross-reactivity of Zika antibodies with other flaviviruses, and nucleic acid and protein biomarkers for ZIKV are detectable at different stages of infection. Here, we describe a new optofluidic approach for the parallel detection of different molecular biomarkers using multimode interference (MMI) waveguides. We report differentiated, multiplex detection of both ZIKV biomarker types using multi-spot excitation at two visible wavelengths with over 98% fidelity by combining several analysis techniques.

OCIS codes: (170.0170) Medical optics and biotechnology; (170.1610) Clinical applications; (130.3120) Integrated optics devices; (230.7390) Waveguides, planar.

References and links

1. G. Kuno, G. J. Chang, K. R. Tsuchiya, N. Karabatsos, and C. B. Cropp, "Phylogeny of the genus Flavivirus," J. Virol. **72**(1), 73–83 (1998).
2. O. Faye, O. Faye, D. Diallo, M. Diallo, M. Weidmann, and A. A. Sall, "Quantitative real-time PCR detection of Zika virus and evaluation with field-caught Mosquitoes," Virol. J. **10**(1), 311 (2013).
3. G. Calvet, R. S. Aguiar, A. S. O. Melo, S. A. Sampaio, I. de Filippis, A. Fabri, E. S. M. Araujo, P. C. de Sequeira, M. C. L. de Mendonça, L. de Oliveira, D. A. Tschoeke, C. G. Schrago, F. L. Thompson, P. Brasil, F. B. Dos Santos, R. M. R. Nogueira, A. Tanuri, and A. M. B. de Filippis, "Detection and sequencing of Zika virus from amniotic fluid of fetuses with microcephaly in Brazil: a case study," Lancet Infect. Dis. **16**(6), 653–660 (2016).
4. A. Galindo-Fraga, E. Ochoa-Hein, J. Sifuentes-Osornio, and G. Ruiz-Palacios, "Zika virus: a new epidemic on our doorstep," Rev. Invest. Clin. **67**(6), 329–332 (2015).
5. C. G. Victora, L. Schuler-Faccini, A. Matijasevich, E. Ribeiro, A. Pessoa, and F. C. Barros, "Microcephaly in Brazil: how to interpret reported numbers?" Lancet **387**(10019), 621–624 (2016).
6. E. Oehler, L. Watrin, P. Larre, I. Leparc-Goffart, S. Lastere, F. Valour, L. Baudouin, H. Mallet, D. Musso, and F. Ghawche, "Zika virus infection complicated by Guillain-Barre syndrome--case report, French Polynesia, December 2013," Euro Surveill. **19**(9), 20720 (2014).
7. D. W. Smith and J. Mackenzie, "Zika virus and Guillain-Barré syndrome: another viral cause to add to the list," Lancet **387**(10027), 1486–1488 (2016).
8. WHO, "WHO to fast-track availability of diagnostics for Zika virus", http://www.who.int/medicines/news/fast_track_diagnostics_zika/en/ (2016).
9. M. T. Osterholm, "Ebola and Zika: Cautionary tales," Science **353**(6304), 1073 (2016).
10. R. S. Lanciotti, O. L. Kosoy, J. J. Laven, J. O. Velez, A. J. Lambert, A. J. Johnson, S. M. Stanfield, and M. R. Duffy, "Genetic and serologic properties of Zika virus associated with an epidemic, Yap State, Micronesia, 2007," Emerg. Infect. Dis. **14**(8), 1232–1239 (2008).
11. J. J. Waggoner and B. A. Pinsky, "Zika virus: diagnostics for an emerging pandemic threat," J. Clin. Microbiol. **54**(4), 860–867 (2016).
12. K. Stettler, M. Beltramello, D. A. Espinosa, V. Graham, A. Cassotta, S. Bianchi, F. Vanzetta, A. Minola, S. Jaconi, F. Mele, M. Foglierini, M. Pedotti, L. Simonelli, S. Dowall, B. Atkinson, E. Percivalle, C. P. Simmons, L. Varani, J. Blum, F. Baldanti, E. Cameroni, R. Hewson, E. Harris, A. Lanzavecchia, F. Sallusto, and D. Corti, "Specificity, cross-reactivity, and function of antibodies elicited by Zika virus infection," Science **353**(6301), 823–826 (2016).

#330752 https://doi.org/10.1364/BOE.9.003725
Journal © 2018 Received 1 May 2018; revised 5 Jun 2018; accepted 13 Jun 2018; published 16 Jul 2018

Biomedical Optics EXPRESS

13. F. Watzinger, K. Ebner, and T. Lion, "Detection and monitoring of virus infections by real-time PCR," Mol. Aspects Med. **27**(2-3), 254–298 (2006).
14. https://www.euroimmun.com/products/indications/infektions-serologie/zika-viruses.html
15. X. Fan and I. M. White, "Optofluidic microsystems for chemical and biological analysis," Nat. Photonics **5**(10), 591–597 (2011).
16. H. Schmidt and A. R. Hawkins, "The photonic integration of non-solid media using optofluidics," Nat. Photonics **5**(10), 598–604 (2011).
17. D. Ozcelik, H. Cai, K. D. Leake, A. R. Hawkins, and H. Schmidt, "Optofluidic bioanalysis: fundamentals and applications," Nanophotonics **6**(4), 647–661 (2017).
18. F. Chiavaioli, P. Zubiate, I. Del Villar, C. R. Zamarreño, A. Giannetti, S. Tombelli, C. Trono, F. J. Arregui, I. R. Matias, and F. Baldini, "Femtomolar detection by nanocoated fiber label-free biosensors," ACS Sens **3**(5), 936–943 (2018).
19. D. Yin, E. J. Lunt, M. I. Rudenko, D. W. Deamer, A. R. Hawkins, and H. Schmidt, "Planar optofluidic chip for single particle detection, manipulation, and analysis," Lab Chip **7**(9), 1171–1175 (2007).
20. J. W. Parks, H. Cai, L. Zempoaltecatl, T. D. Yuzvinsky, K. Leake, A. R. Hawkins, and H. Schmidt, "Hybrid optofluidic integration," Lab Chip **13**(20), 4118–4123 (2013).
21. S. Liu, Y. Zhao, J. W. Parks, D. W. Deamer, A. R. Hawkins, and H. Schmidt, "Correlated electrical and optical analysis of single nanoparticles and biomolecules on a nanopore-gated optofluidic chip," Nano Lett. **14**(8), 4816–4820 (2014).
22. H. Cai, J. W. Parks, T. A. Wall, M. A. Stott, A. Stambaugh, K. Alfson, A. Griffiths, R. A. Mathies, R. Carrion, J. L. Patterson, A. R. Hawkins, and H. Schmidt, "Optofluidic analysis system for amplification-free, direct detection of Ebola infection," Sci. Rep. **5**(1), 14494 (2015).
23. K. Du, H. Cai, M. Park, T. A. Wall, M. A. Stott, K. J. Alfson, A. Griffiths, R. Carrion, J. L. Patterson, A. R. Hawkins, H. Schmidt, and R. A. Mathies, "Multiplexed efficient on-chip sample preparation and sensitive amplification-free detection of ebola virus," Biosens. Bioelectron. **91**, 489–496 (2017).
24. L. B. Soldano and E. C. M. Pennings, "Optical multi-mode interference devices based on self-imaging: principles and applications," J. Lightwave Technol. **13**(4), 615–627 (1995).
25. D. Ozcelik, J. W. Parks, T. A. Wall, M. A. Stott, H. Cai, J. W. Parks, A. R. Hawkins, and H. Schmidt, "Optofluidic wavelength division multiplexing for single-virus detection," Proc. Natl. Acad. Sci. U.S.A. **112**(42), 12933–12937 (2015).
26. H. Cai, M. A. Stott, D. Ozcelik, J. W. Parks, A. R. Hawkins, and H. Schmidt, "On-chip wavelength multiplexed detection of cancer DNA biomarkers in blood," Biomicrofluidics **10**(6), 064116 (2016).
27. D. Ozcelik, A. Jain, A. Stambaugh, M. A. Stott, J. W. Parks, A. Hawkins, and H. Schmidt, "Scalable spatial-spectral multiplexing of single-virus detection using multimode interference waveguides," Sci. Rep. **7**(1), 12199 (2017).
28. D. Ozcelik, M. A. Stott, J. W. Parks, J. A. Black, T. A. Wall, A. R. Hawkins, and H. Schmidt, "Signal-to-noise enhancement in optical detection of single viruses with multi-spot excitation," IEEE J. Sel. Top. Quantum Electron. **22**(4), 4402406 (2016).

1. Introduction

Zika Virus (ZIKV) infection is caused by a mosquito-borne flavivirus [1, 2] and has been strongly correlated with the development of fetal microcephaly and Guillan-Barré syndrome [3–7]. Consequently, the recent 2016 ZIKV outbreak throughout the Americas was declared a public health emergency by the World Health Organization (WHO), and created a pressing need for accelerated development of rapid, specific, and clinically sensitive ZIKV diagnostic techniques [8]. Symptomatic diagnosis of ZIKV in humans is difficult as ZIKV infection can initially present as influenza-like, and can furthermore be easily confused with other flaviviurses, such as Dengue Virus [2]. Currently available tests include qualitative enzyme-link immunosorbent assays (ELISA) which target IgM antibodies and qualitative and endpoint polymerase chain reaction (PCR) assays that measure viral RNA concentrations with amplification-based methods. Due to the recorded cross-reactivity with Dengue Virus, Zika Virus antibody detection is not sufficient as a stand-alone diagnostic tool [2, 9–12], and the involvedness and intricate laboratory setting necessary for PCR tests of nucleic acid targets are non-ideal [13] and limited to nucleic acids. Furthermore, nucleic acid and antibody biomarkers are detectable in different stages of the infection [14]. A biosensor that detects both modalities is, therefore, highly advantageous to accurately diagnose a ZIKV patient and essential to monitoring a possible ZIKV epidemic.

One avenue to accomplish this involves "lab-on-a-chip" devices, which are compact apparatuses that process and analyze clinically relevant chemical or biological samples in small volumes. Optofluidic approaches that integrate photonic principles with biosensing,

Biomedical Optics EXPRESS

bioanalysis, and other applications have produced a number of promising devices [15–18]. Here, we consider a biophotonic analysis platform based on Anti-resonant Reflecting Optical Waveguides (ARROWs) [19]. Orthogonally intersecting liquid-core and solid-core ARROWs allow for planar fluorescence excitation and detection of single biomolecules in flow [17, 20–22, 25–27]. Moreover, these silicon-based chips can be integrated with advanced sample preparation steps on dedicated microfluidic chips, enabling full sample-to-answer analysis of molecular biomarkers on a chip-based system [20, 22, 23, 26].

In order to detect multiple biomarkers simultaneously, we recently introduced a new photonic approach which implements optofluidic wavelength division multiplexing [24–27]. This device is an integrated photonic platform with a multimode interference (MMI) excitation waveguide that supports multiple modes. At well-defined propagation distances, the relative phases of these modes match up to produce clear images which are referred to as spot patterns. Designed properly, different spot patterns can be generated by excitation wavelengths that are matched to the absorption spectra of different fluorescent labels—enabling on-chip spectral multiplexing. Recently, we demonstrated multiplexed fluorescence detection and differentiation of both whole influenza viruses and two blood-borne cell-free nucleic acid melanoma biomarkers on an MMI waveguide-based optofluidic-chip platform [25, 26]. Here, we report the design and implementation of an MMI optofluidic detection scheme that provides a highly specific and sensitive way to detect different types of molecular targets at once. Specifically, dual on-chip detection of Zika virus nucleic acid and protein biomarkers is demonstrated.

2. Principles and methods

We implement the dual detection scheme by simultaneously launching two wavelengths of visible light into a 75 μm wide solid-core excitation waveguide which supports multiple modes with different propagation constants. At well-defined lengths along the waveguide, the relative phases of these modes interfere constructively, creating distinct images, here called spot patterns, which consist of different numbers of images of the original input mode. Here, we design the MMI such that a fluidic microchannel intersects the MMI at a position that corresponds to clear, integer numbers of spots for multiple wavelengths. Figure 1(a) displays a scanning electron microscope (SEM) image of the MMI ARROW chip at the excitation cross section, with a full chip view complete with fluidic reservoirs in the photograph insert (bottom left).

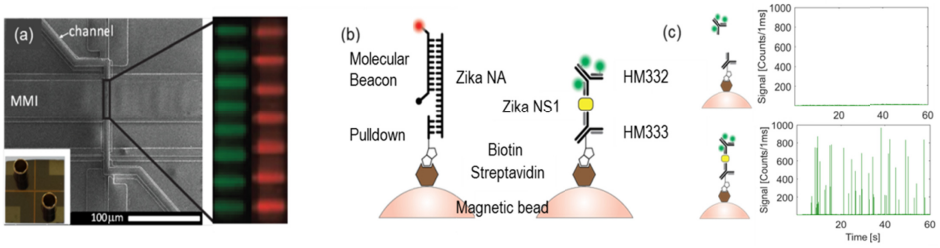

Fig. 1. a) Scanning electron microscope image of fabricated ARROW optofluidic device, with top down multi-mode spot quantum dot images for λ = 556 nm and λ = 633 nm shown on the right, with their respective colors (insert: photo of complete 1cm^2 ARROW optofluidic chip), b) Product from the nucleic acid and protein solid-phase extraction assays used for target isolation with high specificity, c) Particle fluorescence traces detected on ARROW optofluidic chip for the protein detection complex (top: negative control (no NS1 protein); bottom: positive control (with NS1 protein)).

This fluidic microchannel is a liquid-core anti-resonant reflecting optical waveguide (LC-ARROWs) a hollow waveguide that is flanked by dielectric layers that form an anti-resonant Fabry-Perot reflector which enables low loss propagation of light over chip-scale distances

Biomedical Optics EXPRESS

[15]. Single mode fiber is butt-coupled to a single mode excitation waveguide, which launches into the MMI excitation waveguide. Fluorescently tagged targets are directed from an input reservoir to an output reservoir through the LC-ARROW microchannel by pressure-driven flow. As these fluorescent targets pass through the excitation cross-section at the intersection of the LC-ARROW and the excitation MMI waveguide, a fluorescence signal is generated. This fluorescence signal propagates down the LC-ARROW, orthogonal to the excitation waveguide, and is coupled to a collection solid-core waveguide. The signal is then transmitted to and analyzed by an avalanche photodiode (APD). The hollow-core ARROW waveguides were 5 μm x 12 μm in cross section geometry and fabricated using a SU8 sacrificial layer technique and standard planar silicon device fabrication methods [27].

The dependence of the spot number (N) on distance from the beginning of the MMI (L) and the excitation wavelength λ can be derived from standard MMI theory [24] and is given by:

$$N = \frac{n_c w^2}{L\lambda} \tag{1}$$

where w is the effective MMI-WG width (here: 75 μm) and n_c the effective refractive index of the MMI-WG (here: 1.46). When λ = 633 nm; 7 well-defined spots are produced at the MMI length of L = 2243 μm, where the liquid core ARROW intersects the MMI-WG. At the same intersection, choosing λ = 556 nm produces 8 well-defined spots. This provides a means for spectral multiplexing for our targets. Figure 1(a) also shows both excitation patterns of the MMI waveguide within the liquid-core ARROW filled with quantum dots (right).

Target specificity is implemented with a bead-based solid phase extraction method illustrated in Fig. 1(b), which displays the resultant particles for both nucleic acid and protein target isolation. A biotinylated pulldown molecule, either a complimentary oligonucleotide (IDT) specific to a section of the Zika genome or a biotin-functionalized (Roche) ZIKV monoclonal antibody HM333 (East Coast Bio.), was added to streptavidin-coated magnetic microspheres (Thermo) at room temperature for 30 minutes in a medium-high salt solution in accordance with the manufacturer's specifications [12]. The pulldown-functionalized beads were then washed with a low-salt buffer, PBS (Corning). Reporter molecules were then combined with the target nucleic acid (IDT) and target recombinant ZIKV-NS1 protein (East Coast Bio.) and incubated at 37°C for two hours. These reporter molecules were either a complementary nucleic acid probe with TYE665 attached (IDT) or a secondary monoclonal antibody HM332 (East Coast Bio.) functionalized with Cy3 (Lumiprobe). The target and reporter biomarkers were then combined with their respective pulldown beads and left to incubate at room temperature for another 2 hours, at which point they were washed a second time in a low-salt buffer. Each microsphere has the maximum capacity to bind 20 fg of biotinylated antibody or 2.5 x 10^5 molecules of biotinylated ss-oligomer, both of which correspond to a maximum of ~2.4 x 10^5 fluorophores/bead. The isolated target complex is finally pipetted into the input reservoirs of the ARROW chip for detection. Figure 1(c) shows the fluorescence particle trace over time for the protein-bead complex in the absence (top) and presence (bottom) of the NS1 target protein. It is evident from Fig. 1(c) that there is minimal background in the absence of NS1 protein, demonstrating the specificity of this detection scheme for protein detection. This serves as a negative control experiment for our experiments. Specificity for nucleic acid analysis was demonstrated previously in [22, 26].

3. Results and discussion

In Fig. 2, the experimental fluorescence particle trace results for multiplex biomarker detection are shown.

Biomedical Optics EXPRESS

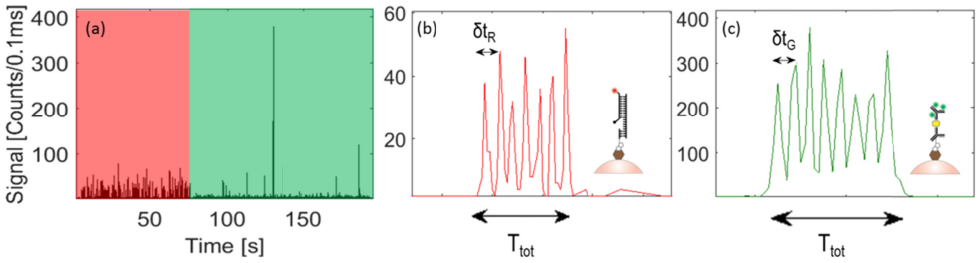

Fig. 2. a) Particle fluorescence trace of both nucleic acid and protein complexes detected in an MMI ARROW chip and excited first with only λ_1 = 633 nm, then with only λ_2 = 566 nm, and finally with λ_1 and λ_2, b) Fluorescence signal from a single nucleic acid complex showing 7 peaks with the signal time (T_{tot}) and characteristic delta t, δt_R = 0.55ms, annotated on the fluorescence signal, c) Fluorescence signal from a single protein complex showing 8 peaks with the signal time (T_{tot}) and characteristic delta t, δt_G = 0.34ms, annotated on the fluorescence signal.

Figure 2(a) depicts the particle fluorescence trace of both the nucleic acid complex and the protein complex. During the first 80 seconds, only the nucleic acid complex is excited on-chip by one laser emitting at λ_1 = 633 nm. The next 90 seconds excite only the protein complex using only a green solid-state laser exciting at λ_2 = 556 nm. Figure 2(b) and Fig. 2(c) show close-ups of single particle fluorescence signals that are identified by their multi-peak pattern—a nucleic acid particle fluorescence signal and protein particle fluorescence signal, respectively. The nucleic acid carrying bead fluorescence signal exhibits a 7 peak pattern, per the design of the MMI, and the protein carrying bead fluorescence single exhibits an 8 peak pattern, also by the design of the MMI waveguide.

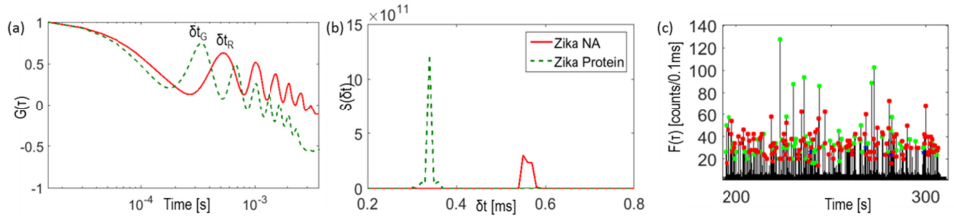

Fig. 3. a) Corresponding single-particle autocorrelation signals for both a red nucleic acid signal and a green protein signal. Multiple peaks are observed at multiples of δt_G, = 0.34 ms and δt_R = 0.55 ms, b) Corresponding enhanced signal using shift-multiply versus δt of the signal shown in (a), signals show an increased SNR when shifted by the correct δt c) Segment of the particle fluorescence trace that was excited with both colors. Events were identified using single particle autocorrelations, shift-multiply algorithms, and total peak duration analysis. Over 98% of signals were identified. Of 215 total signals, 134 were identified as Nucleic Acid complexes, annotated by red squares and 77 were identified as Protein complexes, annotated by green circles.

We employ multiple signal processing methods in order to differentiate the fluorescence particle signals and identify each bead carrying biomarker [28]. With each fluorescence signal pattern, there exists a characteristic time difference, referred to as δt, between each individual peak of the whole signal (see Figs. 2(b) and 2(c)). In the multichromatic trace (see Fig. 3(c)), we extract a characteristic δt for the each of the unidentified peaks by auto correlating each signal and then perform a shift-multiply algorithm to sort it, mentioned below. Figures 3(a) and (b) illustrate this principle. The shift-multiply algorithm we employ is dictated by the equation below:

$$S(t,\ \delta t) = \prod_{m=1}^{N-1} F(t - m \cdot \delta t) \qquad (2)$$

Biomedical Optics EXPRESS

where S(t) is the new, shift-multiplied signal, *N* is the number of MMI spots, F(t) is the particle fluorescence signal, δt is the corresponding characteristic time difference for each individual nucleic acid (red) or protein (green) particle signals, mentioned above [28]. The result is that S(t) is enhanced when the particle trace is shifted the correct number of times (*N*) and by the correct δt, and it is quenched when shifted the incorrect number of times and by the incorrect δt. Figure 3(b) shows enhanced signal values for the signals shown in Fig. 2 (b) and (c) as well as Fig. 3(a). When we perform the shift multiply algorithm, we see that the signals are well separated, and the signal with higher *N* is notably larger as previously reported [28]. Despite a velocity distribution of the ensemble of multichromatic signals, we are able to obtain a velocity-independent confirmation of the fluorescence signal identity using the individual δt of the signal. We also confirmed each peak by vetting with a data parsing scheme that would also mitigate the distribution of velocities in the trace. The spot pattern of the excited particle was directly determined by dividing the total time of the signal by the individual signal's δt, as shown below:

$$N_i = \frac{T_{Tot,i}}{\delta t_i} \tag{3}$$

where N_i is the number of spots created by the MMI excitation of the individual particle, $T_{tot,i}$ is the total time of the individual signal, δt_i is the individual signal's characteristic delta t. In order to robustly identify each particle signal, we applied both methods. If the identity of the particle was verified by both methods, then the particle was defined as such. If there was a discrepancy in the two methods, then the particle was left as unidentified. Figure 3(c) shows implementation of this approach for a fluorescence trace where both lasers are exciting the sample in flow. Of the 215 fluorescence signals in the trace, over 98% were identified. We differentiated 134 red nucleic acid signals and 77 protein signals. We repeated this assay three times with comparable results to ensure repeatability of the approach.

4. Conclusions

We have demonstrated a dual nucleic acid and protein detection scheme using a planar MMI waveguide platform. Zika virus nucleic acid and protein complexes can be excited and detected simultaneously on-chip with high specificity and sensitivity. We demonstrate here that the ARROW optofluidic biosensor is a sample-agnostic platform that is a highly specific and sensitive means of detecting different types of molecular targets at once. The optofluidic platform discussed above can also be incorporated into a dedicated sample preparation and delivery microfluidic layer, as demonstrated in [19, 21, 25]. These results and the upcoming integrated technology show that this optofluidic approach is capable of detecting different classes of biomarkers down to a single antigen using a simple sample preparation and analysis protocol, in contrast with current gold standard techniques such as RT-PCR and ELISA, which are only suited for one type of target.

Funding

W.M. Keck Center for Nanoscale Optofluidics at UC Santa Cruz; NIH (4R33AI100229); National Science Foundation (NSF) (CBET-1159453 and CBET-1159423).

Acknowledgements

We thank J.L. Patterson and R. Carrion Jr. for valuable discussions.

Disclosures

J.W.P., A.R.H., and H.S. have financial interest in Fluxus Inc. which is developing optofluidic devices.